Linear Collider Collaboration Tech Notes

NLC Damping Ring Lattice Design Using TME Cells and Wigglers

17 April 2000

Paul Emma and Tor Raubenheimer
Stanford Linear Accelerator Center
Stanford, CA

Abstract: The design process is described for the damping rings of the Next Linear Collider (NLC) [1]. While the main (e^-/e^+) damping ring is the primary subject, some reference to the (e^+) pre-damping ring is also included. An attempt is made to be systematic in the design, given the emittance and repetition rate requirements of the collider, in conjunction with the beam quality from the injector systems. In addition, qualitative efforts are made to minimize the cost and maximize the dynamic aperture. The approximate interdependencies of the various lattice parameters are derived and arguments for the parameter choices are presented. The rings are a race-track design with wiggler insertions and Theoretical Minimum Emittance (TME) cells. Collective effects and dynamic aperture calculations, while studied in previous designs [**Error! Bookmark not defined.**], are not included here.

NLC Damping Ring Lattice Design Using TME Cells and Wigglers

Paul Emma, Tor Raubenheimer
SLAC

April 17, 2000

ABSTRACT

The design process is described for the damping rings of the Next Linear Collider (NLC) [1]. While the main (e^-/e^+) damping ring is the primary subject, some reference to the (e^+) pre-damping ring is also included. An attempt is made to be systematic in the design, given the emittance and repetition rate requirements of the collider, in conjunction with the beam quality from the injector systems. In addition, qualitative efforts are made to minimize the cost and maximize the dynamic aperture. The approximate interdependencies of the various lattice parameters are derived and arguments for the parameter choices are presented. The rings are a race-track design with wiggler insertions and Theoretical Minimum Emittance (TME) cells. Collective effects and dynamic aperture calculations, while studied in previous designs [1], are not included here.

1 Introduction

There are many parameter choices associated with a damping ring design for a linear collider, such as ring circumference, beam energy, store time, number of bunch trains stored, number of cells per arc, phase advance, and length (or existence) of a damping wiggler. As reasonable design constraints are added, such as cost, dynamic aperture, momentum compaction, alignment tolerances, kicker limitations and spin preservation, and given the beam and timing requirements for the collider, the design choices can be approached systematically. This note describes the approach taken to design the NLC main- and pre-damping rings.

This design procedure is an extension of those described in Refs. [1], [3] and [6]. Based on a few global parameters, such as the injected and extracted emittance and the repetition rate, most of the damping ring parameters can be determined. However, some parameters, such as the energy or number of bunch trains stored, must be initially chosen and then adjusted as the design matures.

The ring circumference is based on the bunch train length and kicker limitations while the store time is a compromise between looser vertical alignment tolerances and unnecessary damping. Beam energy is chosen based on many aspects including spin preservation, reasonable dipole fields, momentum compaction, damping time and wiggler length. A damping wiggler is introduced in order to increase the damping rate without going to a higher, more difficult energy. Finally, the optical design of the TME cells is optimized in order to produce maximum dispersion to improve the dynamic aperture and momentum compaction. The parameter values discussed here are taken mostly from the NLC (e^-/e^+) main damping ring (MDR), but references to the (e^+) pre-damping ring (PDR) are included when useful to illustrate significant differences.

2 Ring Design

The damping ring must produce horizontal and vertical emittances at extraction, which are dictated by the design luminosity. The emittance must also be produced within an inter-pulse period consistent with the machine repetition rate. For the following design, we will assume a 'race-track' ring with two 180°-arcs connected by two long straight sections. The arcs are composed of TME (Theoretical Minimum Emittance) cells [2] which are well suited for a damping ring of this sort.

We first develop a series of equations that relate the choices of ring parameters. The basic NLC parameters that determine the ring's design are given in Table 1 for the (e^-/e^+)

MDR as well as the (e^+) PDR. These values are set by parameters of the collider such as emittance of the injector, collider luminosity and collision repetition rate. Other technical limitations also arise, such as a reasonable rise and fall time of the ring injection and extraction kickers, which means a timing gap must be maintained between stored bunch trains. The large injected emittance of the PDR requires a large aperture kicker so timing requirements have been loosened here.

Table 1. Parameters which determine the minimum circumference and damping requirements of the ring. The values listed here are for the NLC e^+/e^- main damping ring (MDR) and the e^+ pre-damping ring (PDR).

parameter	symbol*	PDR	MDR	unit
number of bunches per train	N_b	95	95	
bunch to bunch spacing within train	t_b	2.8	2.8	nsec
minimum gap between trains for kicker rise/fall	t_k	100	65	nsec
maximum collider repetition rate (of trains)	f	120	120	Hz
injected x and y emittance (norm., rms)	$\gamma\varepsilon_{y0}$	<42000	<150	μm
extraction hor. emittance desired (norm., rms)	$\gamma\varepsilon_x$	<150	<3	μm
extraction ver. emittance desired (norm., rms)	$\gamma\varepsilon_y$	<150	<0.03	μm

* Throughout this note, γ is the electron energy in units of its rest mass.

The design also allows for the simultaneous storing of a number of bunch trains, N_t, which, with the first three parameters in Table 1, determines the minimum ring circumference. The last four parameters determine the damping requirements.

In addition to these parameters the ring must also produce an adequate dynamic aperture, a reasonable rms bunch length (~5 mm) which a compressor system can reduce to ~100 μm, a reasonably large momentum compaction (~5×10^{-4}), and a minimum cost. The cost aspect is addressed here only by attempting to reduce the size and number of components such as the wiggler length, the number of TME-cells, and the number of quadrupole magnets per cell.

2.1 Ring Circumference

The ring's circumference, C, is set by the harmonic number, h, and the RF frequency, f_{RF}, and must be large enough to accommodate the N_t bunch trains, which consist of N_b bunches having a bunch spacing t_b. In addition, a timing gap of t_k between trains is maintained to allow a kicker rise/fall time for injection and extraction. The circumference is then given by

$$C = hc / f_{RF} \geq cN_t T_{train} \quad , \tag{1}$$

where

$$T_{train} = (N_b - 1)t_b + t_k \quad ,$$

and c is the speed of light and h is the harmonic number. For the NLC main damping ring, as will be seen, $N_t < 3$ sets the circumference too small for reasonable magnet strengths and $N_t > 3$ generates a larger circumference than necessary. At $N_t = 3$, and the parameters of Table 1, the MDR circumference must satisfy $C \geq 295.27$ m. Assuming an rf frequency of $f_{RF} = 714$ MHz and $h = 708$ (evenly divisible by 2, 3, or 4 bunch trains) the circumference of the MDR is $C = 297.273194$ m.

2.2 Vertical Emittance and Store Time

For a flat beam, achieving the very small extracted vertical emittance is the most challenging aspect of ring design and construction. Many of the most demanding tolerances, such as sextupole and quadrupole magnet alignment, are set by the chosen equilibrium vertical emittance, e_{ye}. The extracted vertical emittance is a combination of the damped injection emittance and the error-driven equilibrium emittance,

$$e_y = e_{y0}e^{-2N_t} + \left(1 - e^{-2N_t}\right)e_{ye}, \tag{2}$$

where N_t is the store time per train in units of damping time constants ($N_t \equiv \Delta t / t_y$) and the other symbols are described above or in Table 1. For given values of injection and extraction emittance, the choice of equilibrium emittance is a balance between looser vertical alignment tolerances (*i.e.* large e_{ye}) and a longer relative store time (*i.e.* large N_t).

$$\frac{e_{ye}}{e_y} = \frac{e^{2N_t} - e_{y0}/e_y}{e^{2N_t} - 1} \tag{3}$$

Loosening vertical alignment tolerances amounts to increasing the equilibrium emittance, e_{ye}, toward the extracted emittance, e_y. Figure 1 shows the ratio of equilibrium emittance to extracted emittance, e_{ye}/e_y, (plotted for $ge_y = 0.03$ mm) versus relative store time, N_t [see Eq. (3)]. The point at which e_{ye}/e_y crosses zero is not important. It is simply the number of damping times where it is impossible to achieve a value of $ge_y = 0.03$ mm, from the given initial emittance.

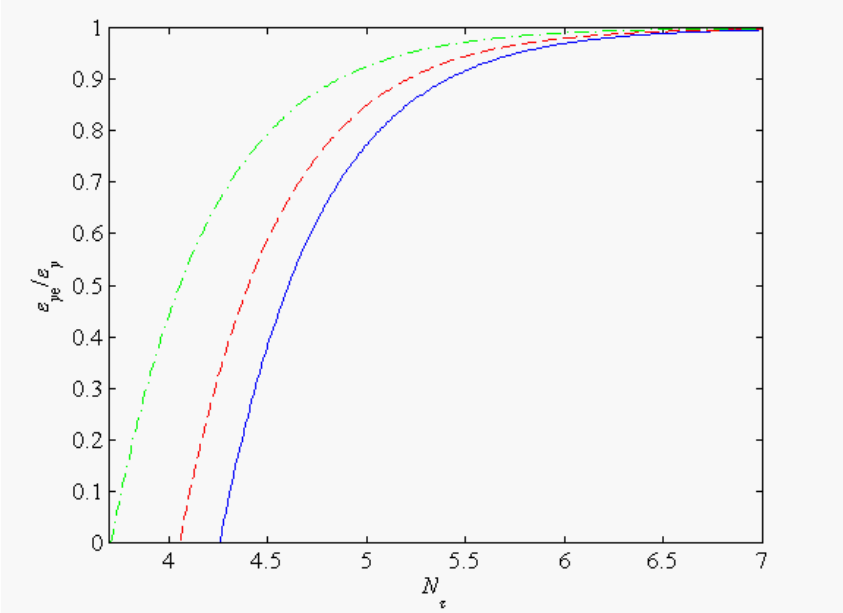

Figure 1. Equilibrium vertical emittance divided by an extracted emittance of $ge_y = 0.03$ *m*m, versus relative store time, N_t for initial emittance values of $ge_{y0} = 150$ *m*m (solid), 100 *m*m (dash), and 50 *m*m (dot-dash). A reasonable choice that adequately loosens tolerances is in the region $0.6 < e_{ye}/e_y < 0.9$.

As seen in Figure 1, increasing N_t eventually has no significant effect on e_{ye}/e_y. Since the vertical alignment tolerances scale with $e_{ye}^{1/2}$, it seems reasonable to choose $0.6 < e_{ye}/e_y < 0.9$. Choosing larger values forces a faster damping rate with little benefit in terms of alignment tolerances. Choosing much smaller values tightens the tolerances unnecessarily. The choice for the NLC main damping ring is made, somewhat arbitrarily, at $e_{ye}/e_y \approx 0.67$. This choice attains tolerances which are just 18% tighter than for $N_t \to \infty$, and sets $N_t = 4.8$ and $ge_{ye} \approx 0.02$ *m*m for an initial emittance of $ge_{y0} \approx 150$ *m*m. This argument is not valid in the PDR with the much larger emittance and looser alignment tolerances. Even for $e_{ye}/e_y \approx 0.1$, the equilibrium emittance is $ge_{ye} \approx 15$ *m*m and alignment tolerances are $(15/0.02)^{1/2} \approx 30$-times looser (*i.e.* of order 1 mm rather than 30 *m*m [3]). Because the alignment is not an issue in the PDR, a smaller value of N_t (≈ 3.1), and therefore a simpler ring, can be accepted by choosing $e_{ye}/e_y \approx 0.1$ in the PDR.

A further reason to limit the upper range of N_t in the MDR is due to the emittance limit given by the opening angle, g^{-1}, of the synchrotron radiation. The damped vertical emittance is limited to [4]

$$\Delta ge_y \approx 0.24 \cdot J_e \langle b_y \rangle \frac{s_d^2}{g}, \tag{4}$$

where J_e (≈ 2) is the longitudinal damping partition number, $\langle b_y \rangle$ (≈ 5 m) is the mean vertical beta function, and s_d (≈ 0.1 %) is the rms relative energy spread. For typical values (in parentheses) at 2 GeV, this emittance limit is $\Delta ge_y \approx 0.0005$ *m*m, or 2% of the

desired MDR extraction emittance. At $N_t \approx 6.3$ an initial emittance of $\gamma\varepsilon_{y0} \approx 150$ mm will damp to 0.0005 mm, equal to the minimum emittance determined the opening angle of the radiation, which implies that such a long store time is probably not useful.

2.3 Damping Time and Beam Energy

The required store time, Δt (= $N_t t_y$), is a function of the ring bends [5] and should be shorter than the time between machine pulses (*i.e.* trains), $1/f$, increased by the number of stored bunch trains, N_t.

$$t_y = \frac{3C}{r_e c \gamma^3 I_2} \le \frac{N_t}{f N_t} \tag{5}$$

Here r_e is the classical electron radius, c is the speed of light, and I_2 (= $\Sigma_i \ell_i / r_i^2$) is the 2nd synchrotron integral over the length, ℓ_i, and radius, r_i, of each bend. For $N_t = 3$, $N_t = 4.8$ and the MDR parameters of Table 1, the damping time constant, t_y, must be less than 5.2 ms. For an isomagnetic ring without wigglers, the damping time is approximately given by

$$t_y \approx \frac{(2.89\times10^{12}\ \text{kG})C}{B_a \gamma^2 c}, \tag{6}$$

where C is the circumference from Eq. (1), and B_a is the bend field of the arc dipole magnets in kG.

Note that when damping multiple trains of bunches at the same time, the damping time *per se* is not the relevant parameter. Instead, we are concerned with the damping time scaled by the number of bunches in the ring which is roughly proportional to the ring circumference; two rings, one with twice the damping time but storing twice as many trains, will have the same damping performance. The damping requirement Eqs. (5) and (6) can be re-written in terms of a 'effective' damping time which is independent of the ring circumference and only depends of the bunch train length and the separation between the trains,

$$\frac{t_y}{N_t} \equiv t_{eff} \approx \frac{(2.89\times10^{12}\ \text{kG})T_{train}}{B_a \gamma^2} \le \frac{1}{f N_t}, \tag{7}$$

where T_{train} and N_t are described in Section 2.2.

According to Eq. (6), to achieve $t_y < 5.2$ ms with $C \ge 295.27$ m, the MDR energy must be $\gamma mc^2 \ge 2.83$ GeV such that the dipoles are non-superconducting magnets with $B_a \approx 18$ kG. For other reasons to be discussed in Section 2.6, the energy is chosen at 1.98 GeV. The damping time is then achieved by adding wiggler magnets to the straight sections (see next section).

2.4 Wiggler Damping

Introducing a wiggler magnet into the ring generates more damping (*i.e.* an additive component to the I_2 synchrotron integral). With the definition

$$F_w \equiv I_{2w}/I_{2a} \geq 0, \tag{8}$$

where I_{2w} is the sum $\Sigma_i \ell_i/r_i^2$ over the wiggler bends and I_{2a} is this sum over the arc bends, the damping time can be rewritten as

$$t_{eff} \approx \frac{(2.89\times10^{12}\ \text{kG})T_{train}}{B_a g^2(1+F_w)}. \tag{9}$$

The factor F_w represents the relative damping in the wiggler compared to that of the arcs. A ring without wiggler has $F_w = 0$, and for $F_w = 1$ the damping (or energy loss per turn) is equally shared by the arcs and wiggler. For $F_w > 1$ the damping is dominantly achieved in the wiggler. A damping time of $t_y < 5.2$ msec ($t_{eff} < 1.7$ msec) is achieved in the MDR at 1.98 GeV with $B_a < 18$ kG if $F_w > 1$. The second synchrotron integral in the arcs, I_{2a}, can be derived from the definition of I_2 and assuming an isomagnetic ring with a total of $2p/q$ bends each of bend angle q.

$$I_{2a} = \frac{2p\,B_a}{(Br)} \tag{10}$$

Here (Br) is the standard energy dependent magnetic rigidity. The second synchrotron integral in the wiggler, I_{2w}, can be written from the definition of I_2 and assuming a hard-edged wiggler field of B_w with dipoles occupying half the wiggler length.

$$I_{2w} \approx \frac{L_w B_w^2}{2(Br)^2} \tag{11}$$

The active length of wiggler required for an isomagnetic arc is then taken from Eq. (5) with $I_2 = I_{2a} + I_{2w}$ and Eqs.(8), (10) and (11).

$$L_w \approx \frac{6C(Br)^2}{r_e c t_y g^3 B_w^2} \cdot \frac{F_w}{1+F_w} \tag{12}$$

Note that the wiggler peak field is the same for a hard edge model or a sinusoidal model when the integral over the square of the field is held constant (*i.e.* I_{2w} is held constant). Equation (12) shows that the wiggler length reaches an asymptotic value for $F_w >> 1$, in which case the wiggler does all the damping and the arcs do none. For the MDR parameters listed above at 1.98 GeV and $B_w = 21.5$ kG, a maximum wiggler length (*i.e.* $F_w \to \infty$) of $L_w \approx 66$ m is required. Conversely, the minimum length is 33 m at $F_w = 1$. Before choosing a value for F_w, its effect on other parameters, including emittance and momentum compaction must be considered.

2.5 Horizontal Emittance

For a flat extracted beam, $e_y << e_x$, and several damping times, $N_t > \ln(e_{x0}/e_x)$, the injected horizontal emittance is typically damped to an insignificant level with respect to the equilibrium horizontal emittance. In this case the equilibrium emittance is effectively the same as the extracted emittance and we can therefore ignore the injected horizontal emittance in what follows.

This section follows the arguments presented in reference [6] concerning the equilibrium horizontal emittance of a TME (theoretical minimum emittance) cell. The TME cell is composed of one bend of length L and angle q and several (typically 3~4) quadrupole magnets. In our case, the bend magnets have no field gradient. This makes the bends less costly, easier to design and fabricate, and transverse alignment is not an issue [7].

The cell's horizontal beta, b, and dispersion, h, functions reach a minimum in the center of the bend. The horizontal equilibrium emittance generated in a ring can be written as [5]

$$ge_x = \frac{C_q g^3 I_5}{J_x I_2}, \tag{13}$$

where $C_q \approx 3.84\times10^{-13}$ m, J_x (= $1 - I_4/I_2$) is the horizontal partition, and I_4 and I_5 are the 4th and 5th synchrotron integrals, respectively [5]. This can be written (as a proportionality) using the effective damping time in a form that more explicitly illustrates the constraints,

$$ge_x \propto \frac{I_5 T_{train}}{t_{eff}(J_x + F_w)}, \tag{14}$$

where the train length and effective damping are specified by the performance requirements of the ring and J_x and the I_5 integral depend on details of the specific lattice.

2.6 Ring Energy

There are a number of considerations when determining the ring energy. First, the desire to maintain high-spin polarization while damping the beams suggests that the nominal ring energy should be chosen so that the spin tune is a half integer. This limits the energy as

$$ag = n + \frac{1}{2}, \tag{15}$$

to minimize the electron beam depolarization. Here, $a \equiv (g-2)/2 \approx 1.16\times10^{-3}$ is the anomalous magnetic moment of the electron. At an energy $gmc^2 \approx 1.98$ GeV, the condition is met with $n = 4$.

Second, we would prefer to keep the ring energy low in order to reduce ring costs as well as keeping the normalized longitudinal emittance small, making the bunch compression easier.

The problem with a low-energy ring is that it is harder to attain the required damping using reasonable magnet designs. We can understand the choices using the previous formulas. First, using Eqs (9) and (12) and assuming that the fraction of damping due to the wigglers, F_w, and the wiggler peak field, B_w, are fixed, we find that, to meet the damping time requirements, the main bending field and the required length of wiggler scale as

$$B_a \propto \frac{1}{g^2} \quad \text{and} \quad L_w \propto \frac{1}{g} \ . \tag{16}$$

Thus, as the ring energy is increased, the bending magnets and wigglers become easier to design and construct.

Next, using Eq. (14) and noting that the I_5 integral scales as $I_5 \propto q^3/r$, we find that, to maintain the equilibrium emittance, the number of cells, N_c, and the bend magnet length, L, scale as

$$N_c \propto g \quad \text{and} \quad L \propto g^2 \ . \tag{17}$$

Finally, given these relations, the circumference of the ring, the momentum compaction, and the synchrotron radiation power must scale as

$$C \propto g^3 \quad \text{and} \quad a_p \propto \frac{1}{g^2} \quad \text{and} \quad P_{SR} \propto U_0 \propto g \ , \tag{18}$$

where we assume that the cell length scales in the same manner as the length of the bends. The cost of the rings will tend to increase with the length, while the cost of the rf systems will increase with the power required; both of these costs will increase with higher energy. In addition, the momentum compaction decreases with the square of the ring energy while rough scaling for the longitudinal microwave threshold scales as ga_p. This suggests that longitudinal stability may be more difficult at higher energy.

Thus, the determination of the nominal ring energy becomes an optimization between the difficulty of the bending and wiggler magnets versus the decrease in momentum compaction, and the increase in size and cost of the ring. We have picked an energy of 1.98 GeV and a spin tune of 4.5. This is the lowest energy that appears to yield reasonable designs for the bending magnets and wigglers. Of course, during operation, we may want to vary the ring energy to optimize for a lower repetition rate or a larger

injected emittance. For this reason, we are designing the rings to operate over the 1.9—2.1 GeV range.

Finally, it is worth noting that intrabeam scattering does *not* present justification for increasing the ring energy. *When the effective damping times are held constant*, the emittance growth due to intrabeam scattering does not decrease with the ring energy. Using a very simple scaling formula, the emittance growth depends upon the intrabeam scattering growth rate compared to the synchrotron radiation damping. The intrabeam scattering growth rate scales roughly as

$$t_{IBS}^{-1} \propto \frac{N\langle H\rangle}{\gamma\varepsilon_x\gamma\varepsilon_y\gamma\varepsilon_z} \ , \tag{19}$$

where N is the number of particles per bunch and $\langle H\rangle$ is the average of the dispersion invariant around the ring. The dispersion invariant scales as $\langle H\rangle \propto \gamma^3 r$ which, because the bending magnet field scales inversely with γ^2 while the number of cells increases with γ, as discussed in Eqs. (16) and (17), will be independent of energy. Thus, for given normalized emittances, the intrabeam scattering rate is independent of energy. In contrast, the damping rates are proportional to the effective damping times divided by the ring circumference [Eq. (7)]. Since the ring circumference increases as γ^3 [Eq. (18)], the damping rates scale inversely with γ^3. Finally, because the emittance growth due to intrabeam scattering depends on the scattering growth rate compared to the damping rate, the intrabeam scattering actually becomes worse as the design energy is increased!

2.7 Lattice Choices

At this point, we should discuss the various lattice options. To attain the very low emittances needed in a future collider, the lattice should be efficient and have a small I_5 integral for a given bending magnet strength. Many possible lattice choices have been developed for the low emittance synchrotron radiation sources including the Triple Bend Achromat (TBA) and the Chasman-Green lattice. We will summarize the advantages and disadvantages of these lattices along with the TME lattice and the FOBO lattice which is a modified FODO lattice, where the defocusing quadrupole is replaced with a combined function bending magnet.

- FOBO
  - \+ Simple FODO-like structure with well constrained β-functions
  - – Uses three quadrupoles per bending magnet
  - – Less efficient at generating emittance
  - – Requires difficult combined function bending magnet
- Chasman-Green

  - \+ Fairly efficient at generating emittance
  - \+ Uses two quadrupoles per bending magnet
  - \+ Presently used at ESRF and ELETTRA
- TBA
  - \+ Fairly efficient at generating emittance
  - \+ Uses two quadrupoles per bending magnet
  - \+ Presently used at ALS and PLS
- TME
  - \+ Very efficient at generating emittance
  - \+ Easy to optimize emittance and momentum compaction
  - – Uses three or four quadrupoles per bending magnet

The needs of the damping rings are slightly different from that of the SR sources. In particular, one does not need many dispersion-free straight sections for insertion devices. In the damping rings, we need one dispersion-free region for injection and extraction and possibly another for a damping wiggler. The Chasman-Green and the TBA lattice were originally designed to have dispersion-free straight sections after every pair or every triplet of bending magnets, respectively. Although recently the lattices are sometimes re-optimized to attain better emittance performance by allowing dispersion between achromat cells, the lattices are not really optimized to create compact and efficient 180° arcs consisting of many cells. For this reason, we will only consider the TME lattice for the damping rings.

Another consideration is the choice of the horizontal damping partition number J_x. By using a combined function bend with a defocusing gradient, it is possible to reduce the equilibrium horizontal emittance and increase the horizontal damping rate. However, combined function magnets are more difficult to align and have tighter field tolerances. Furthermore, as can be seen by examining Eq. (14), if the wiggler damping parameter F_w is significantly greater than zero, the relative gain from changing J_x is small. For this reason, we would only choose to use a combined function magnet if it simplifies the matching of the cell, which it does not. The present design is based on separated function magnets.

2.8 TME Lattice

For a TME-cell with small angle bends ($q << 1$) and optical symmetry with respect to the middle of the bend magnet (*i.e.* $dh/ds = db/ds = 0$ at bend center), the equilibrium emittance is, from Eq. (13),

$$ge_x \approx \frac{C_q g^3}{J_x}\left[\frac{h^{*2}}{b^* L}q - \frac{h^*}{12b^*}q^2 + \left(\frac{b^*}{12L} + \frac{L}{320b^*}\right)q^3\right], \qquad (20)$$

where b^* and h^* are the horizontal beta and dispersion functions at the center of the bend of length L. The emittance is minimum, ge_{x_m}, for an optimal set of functions, b_m^* and h_m^* [2] given by

$$b_m^* = \frac{L}{2\sqrt{15}}, \qquad h_m^* = \frac{Lq}{24}, \qquad ge_{x_m} \approx \frac{C_q g^3}{J_x} \frac{q^3}{12\sqrt{15}}. \tag{21}$$

The cell is then 'detuned', with respect to this optimum, in order to increase the dispersion function, which will reduce the strengths of the chromatic correction sextupoles and potentially increase the ring's dynamic aperture. The unitless 'detuning' factor, $e_r \equiv e_x / e_{x_m} \geq 1$, is expressed as a function of the relative optical functions $b_r \equiv b^*/b_m^*$ and $h_r \equiv h^*/h_m^*$ [6].

$$e_r = \frac{5}{8}\frac{h_r}{b_r}[h_r - 2] + \frac{9}{2}\left[\frac{1}{4b_r} + \frac{b_r}{9}\right] \tag{22}$$

Eq. (22) is plotted on a log-log scale in Figure 2 (as in reference [6]) as h_r versus b_r for five different values of the relative emittance, e_r (= 2, 4, 8, 16, and 32).

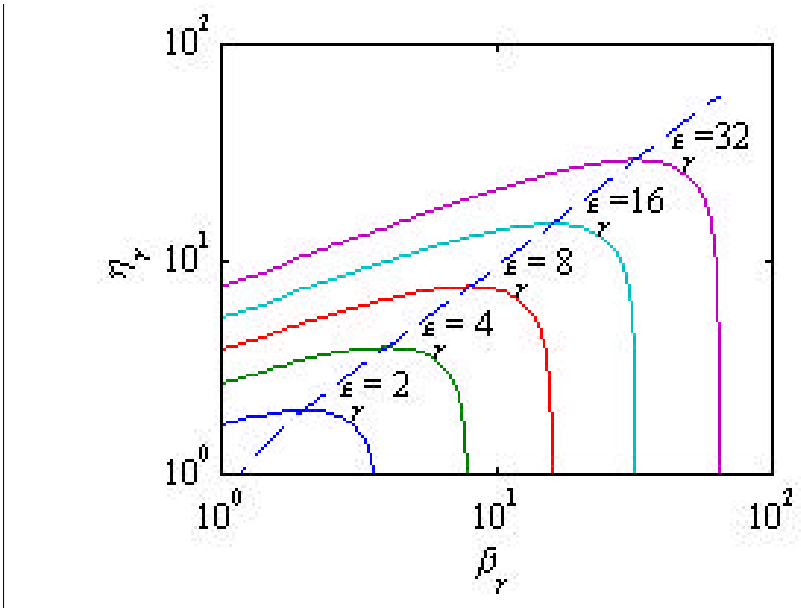

Figure 2. Relative dispersion, h_r, versus relative beta function, b_r, at center of bend in TME cell [6] for five different values of the emittance detuning factor, e_r (= 2, 4, 8, 16, and 32). The dashed curve follows the maximum values of h_r and relates to Eq. (23).

From Figure 2, a maximum in h_r can be found at a unique value of b_r for a given value of e_r. With h_r maximized (*i.e.* $dh_r/db_r = 0$) the optimal relative functions and detuned emittance scale with e_r as

$$b_r = e_r \ , \qquad h_r = 1 + \frac{2}{\sqrt{5}}\sqrt{e_r^2 - 1} \ , \qquad ge_x \approx e_r \frac{C_q g^3}{J_x} \frac{q^3}{12\sqrt{15}} , \tag{23}$$

and the maximum value of h_r moves along the dashed line of Figure 2 for different values of e_r. The functions required in the bend center are then given from Eqs. (21) and (23) as

$$b^* = e_r \frac{L}{2\sqrt{15}} \ , \qquad h^* = \frac{Lq}{24}\left[1 + \frac{2}{\sqrt{5}}\sqrt{e_r^2 - 1}\right]. \tag{24}$$

The detuning factor is chosen only after consideration of its impact on other ring parameters, such as momentum compaction, which will be described. Finally, the required emittance is attained by choosing the appropriate bend angle q in Eq. (23) and, for a simple race-track ring, the number of TME-cells required *per arc* is set by $N_c = p/q$.

2.9 Emittance Detuning Factor and Phase Advance

By calculating the propagation of the periodic dispersion and its angle from the cell border to bend center, and including the conditions $h' = 0$ at both boundaries and $h = h^*$ at bend center, the detuning factor, e_r, can be shown [8] to be uniquely given by the horizontal phase advance per ½-TME cell, m_x.

$$\tan m_x = \frac{\sqrt{3} e_r}{\sqrt{e_r^2 - 1} - \sqrt{5}} \tag{25}$$

Thus a phase advance per ½-TME cell of $m_x \approx 142°$ produces the smallest emittance of $e_r = 1$. A value of $e_r = \sqrt{6}$ is produced with a 90° per ½-cell phase advance. Similarly, as $e_r \to \infty$, the phase advance per ½-cell approaches 60°. Figure 3 summarizes this relationship. Therefore, in choosing the emittance detuning factor we are simply choosing the horizontal phase advance per ½-cell. The specific choice of values for e_r is reserved for the next sections where its impact on other ring characteristics is studied.

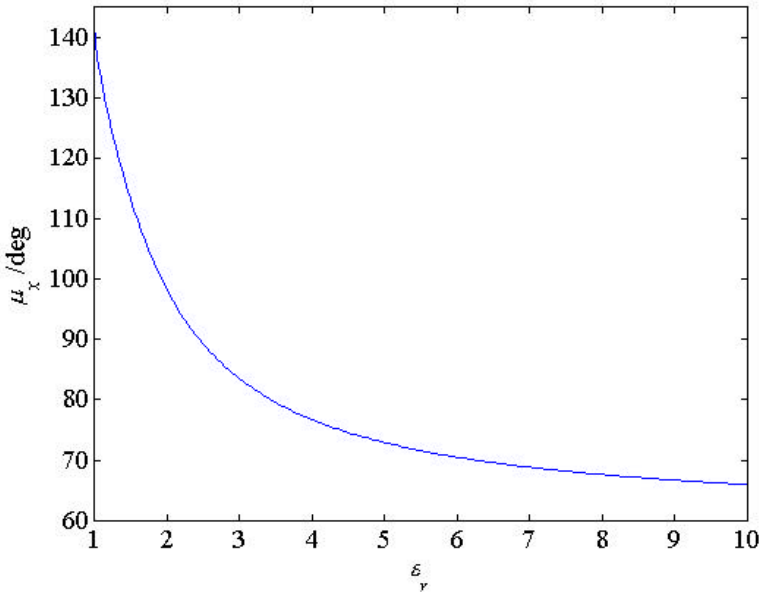

Figure 3. Horizontal phase advance per ½-TME cell as a function of the emittance detuning factor, e_r.

2.10 Horizontal Emittance with a Wiggler

The addition of a wiggler increases the damping rate and adds a component to the equilibrium emittance. By expanding the I_2 and I_5 synchrotron integrals in Eq. (13), the net equilibrium emittance of the ring is written as

$$ge_x \approx ge_a \cdot \frac{J_{x0}}{J_{x0} + F_w} + ge_w \cdot \frac{F_w}{J_{x0} + F_w}, \tag{26}$$

for a typical wiggler with bend angle per half-period $q_w << 1$. Here ge_a is the equilibrium emittance produced by the arcs in the absence of a wiggler [given by Eq. (23)], ge_w is the emittance produced by the wiggler for $F_w \to \infty$, and J_{x0} is the horizontal damping partition number of the arcs (without a wiggler). With no field gradient in the arc dipoles: $J_{x0} \approx 1$.

The emittance produced by the wiggler can be approximately calculated using Eq. (13) and a hard-edged wiggler field model with period l_w, and peak field B_w.

$$ge_w \approx C_q g^3 \frac{B_w^3 l_w^2 \langle b_x \rangle}{192(Br)^3}, \tag{27}$$

The average horizontal beta-function, $\langle b_x \rangle$, through the wiggler is used here and assumed to fit the trivial condition $\langle b_x \rangle >> l_w/2p$. Substituting into Eq. (26) for ge_a and ge_w from Eq. (23) and (27), respectively, gives the net horizontal equilibrium emittance of the ring, including wiggler.

$$ge_x \approx \frac{C_q}{12(J_{x0}+F_w)}\left[\frac{e_r g^3 q^3}{\sqrt{15}}+\frac{F_w B_w^3 l_w^2 \langle b_x\rangle}{16}\left(\frac{g}{(Br)}\right)^3\right] \tag{28}$$

This approximation ignores the details of the dispersion suppressor optics at the start and end of the arcs, but is still a fairly accurate description, especially when the number of TME-cells per arc is large (*e.g.* >10).

Note that the wiggler component of the emittance varies with the cube of its peak field and the square of its period. Since the length of the wiggler also varies inversely with the square of its peak field [see Eq (12)], a weak field is not an advantage. However, reducing the wiggler period, within reasonable field limits, is useful. The Halbach scaling for hybrid wigglers [9] describes a limit on the peak field, B_w, in terms of the ratio of the wiggler full-gap, g, to wiggler period

$$B_w[kG] \le 34.4\exp\left[-\frac{g}{l_w}\left(5.08-1.54\frac{g}{l_w}\right)\right], \tag{29}$$

which is roughly valid over the interval $0.08 < g/l_w < 0.7$. At a value of $g/l_w \approx 0.08$ the peak field might achieve 21.5 kG. This means that a gap of $g \approx 2$ cm requires a period of $l_w \approx 25$ cm. This relationship is only used as a starting point. The details of a realistic wiggler design constitute a separate study.

The mean beta function, $\langle b_x\rangle$, through the wiggler can be kept reasonably small by segmenting the wiggler and adding quadrupole magnets at the segment gaps. The mean beta function is then approximately twice the length of these modular wiggler segments (for a 90°/cell wiggler FODO lattice). It is therefore useful to keep the lengths of the wiggler segments relatively short (*e.g.* 2 m) and maintain a horizontal phase advance in the region of ~90°/cell through the wiggler using a FODO-cell lattice. With multiple FODO cells the ring tunes are easily varied over a significant range by adjusting the phase advance per cell of the wiggler focusing lattice. Maintaining a range of approximately 90~120°/cell in ten cells then allows a horizontal tune adjustment range of ±0.4 without a significant variation in the horizontal emittance. The vertical tune adjustment can be even larger. Figure 4 shows the relative horizontal equilibrium emittance of an example NLC MDR ring as a function of horizontal phase advance per wiggler FODO-cell calculated using MAD [10]. A phase advance per wiggler FODO cell of 108° is about the minimum.

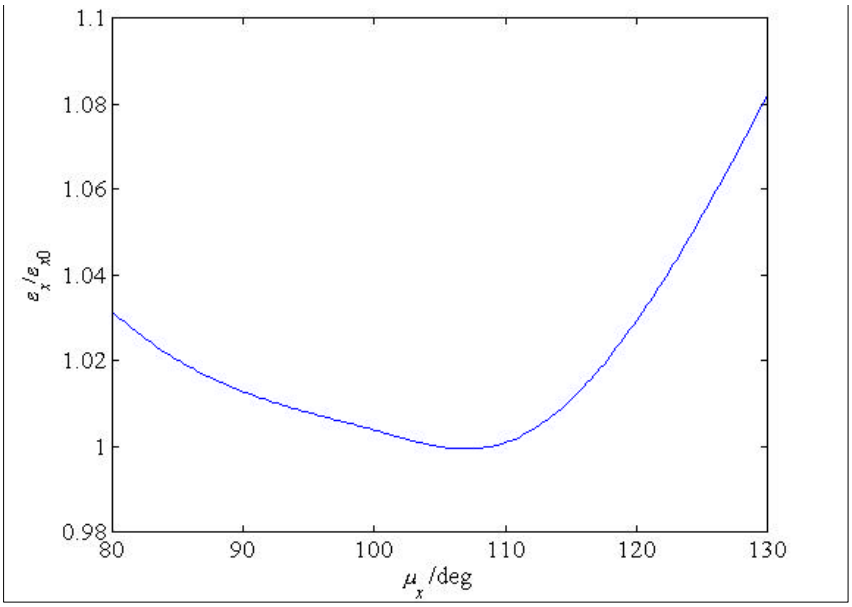

Figure 4. Relative horizontal emittance as a function of horizontal phase advance per wiggler FODO-cell calculated with MAD [10]. The vertical phase advance per FODO-cell is held constant at $m_y = 72°$ and $ge_{x0} = 3$ *m*m.

2.11 TME-Cell Design

The bend angle of a TME-cell dipole magnet is given by Eq. (28) solving for q, and requiring $?e_x = 3$ μm. The number of TME-cells required per arc, N_c, is then set by the racetrack design as $N_c = p/q$.

$$N_c \approx pg\left(\frac{e_r}{\sqrt{15}}\right)^{1/3}\left[\frac{12g\,e_x}{C_q}\left(J_{x_0}+F_w\right)-\frac{F_w B_w^3 l_w^2\langle b_x\rangle}{16}\left(\frac{g}{(Br)}\right)^3\right]^{-1/3} \tag{30}$$

The number of cells per arc is kept small by choosing small e_r (shown in Figure 7). The cell is composed of 3 or 4 quadrupoles and one dipole magnet. The dipole field, B_a, is given by Eq. (9) and its bend angle, q, is based on the emittance in Eq. (28), so the length of the dipole magnet is uniquely defined by $L = q(Br)/B_a$. The values for b^* and h^* are given by Eq. (24) and the cell drift lengths and quadrupole strengths (one focussing and one de-focussing family) are solved for in a non-linear fit to produce the necessary values for b^* and h^* in the bend center. Figure 5 shows an example 3-quad TME-cell and its optical functions for the MDR with magnet locations graphically depicted at top. The bend magnet is in the center of the plot (for this plot: $D_x \equiv h$) and the phase advance per ½-cell is $m_x = 108°$ and $m_y = 36°$. (A ratio of $m_x/m_y \approx 3$ is assumed favorable for dynamic aperture.)

Figure 5. Optical functions of a 3-quad TME-cell for the NLC MDR with bend at center (note $D_x \equiv h$). Magnet layout is indicated at top with the bend at center and quadrupoles shown larger than sextupoles.

The pre-damping ring (PDR), with its very large injection emittance, is better suited to a 4-quad TME-cell. The 4-quad cell produces smaller beta function peaks and thus leads to a smaller peak beam size. Figure 6 shows a 4-quad TME-cell for the PDR where the vertical beta function peaks at ~32 m rather than >60 m in a similar 3-quad design.

Figure 6. Optical functions of a 4-quad TME-cell for the NLC PDR.

It is also possible to generate a TME-cell with quadrupole gradients reversed from those indicated in Figure 5 and Figure 6. The reversed polarity cell has horizontally defocusing magnets located near the bend. Such cells have been applied to the MDR and generally produce weaker quadrupoles and larger dispersion in the nearby sextupoles. This may be an advantage for increasing the dynamic aperture, but the cells are limited in achievable horizontal phase advance (or detune factor). Since the horizontal beta functions in the reversed cell increases monotonically from bend center to cell boundary, as opposed to that of Figure 5, the horizontal phase advance is limited to approximately 90° per ½-cell [11]. This limits e_r in the reversed cell to ≈2.5 which requires ≈35 % more TME-cells than for $e_r = 1$ [see Eq. (30)]. The reversed polarity cell is therefore not used here.

Each arc is composed of $N_c - 1$ *full* length cells plus a half-cell to start and another half-cell to terminate the periodic dispersion function in the arc. The half-cells are dispersion suppressors, include one half-length bend, and are slightly modified from a perfect half-cell in order to precisely match the periodic dispersion function of the arc. The length of a full cell is determined from the ring circumference, the number of cells per arc in Eq. (30), and the straight section length needed to comfortably fit the wiggler of Eq. (12). Short, adjustable beta-matching sections separate the straight sections from the dispersion suppressors. The final value for the phase advance per TME ½-cell is determined by e_r, which is chosen based on arguments presented in the next section.

2.12 Momentum Compaction

Another goal of the design is to keep the momentum compaction, a_p, of the ring relatively large to avoid instability thresholds. For the NLC MDR design, a somewhat arbitrary goal of $a_p \geq 5\times10^{-4}$ has been set. The momentum compaction is given by [5]

$$a_p = I_1/C\,, \tag{31}$$

where I_1 ($= \Sigma_i \ell_i \langle h \rangle_i / r_i^2$) is the 1st synchrotron integral, C is the nominal ring circumference, and $\langle ? \rangle_i$ is the mean dispersion function averaged over the length of the bend magnet. Using the mid-point dispersion, h^*, from Eq. (23), and the bend angle solved with Eq. (28) gives

$$a_p \approx p^2 \left(\frac{4\sqrt{15}}{9}\right)^{2/3} \frac{r_e c t_y g (1+F_w)^{5/3}}{C^2} \left(\frac{g e_x}{C_q} - \frac{B_w^3 l_w^2 \langle b_x \rangle g^3}{192(Br)^3} \frac{F_w}{J_{x0}+F_w}\right)^{2/3} \frac{\sqrt{5}+\sqrt{e_r^2-1}}{e_r^{2/3}}\,. \tag{32}$$

The momentum compaction is a function of e_r as shown in Figure 7, where it is also clear that $e_r > 4$ amounts to ≈60% more TME-cells than at $e_r = 1$. The maximum momentum compaction, for a reasonable number of TME-cells, is then located at $e_r \approx 1.3$. To keep the momentum compaction large without adding a significant number of costly TME cells requires choosing e_r near this peak. Eq. (25) shows that $e_r = 1.647$ is equivalent to a horizontal phase advance per ½-cell of $m_x \approx 108°$. This judicious choice allows five TME-cells to produce 6p of phase advance and, therefore, sextupole aberrations are more locally cancelled by optical symmetry. For these reasons we choose $e_r = 1.647$ which produces $a_p/a_{p0} \approx 1.14$ and $N_c/N_{c0} \approx 1.18$.

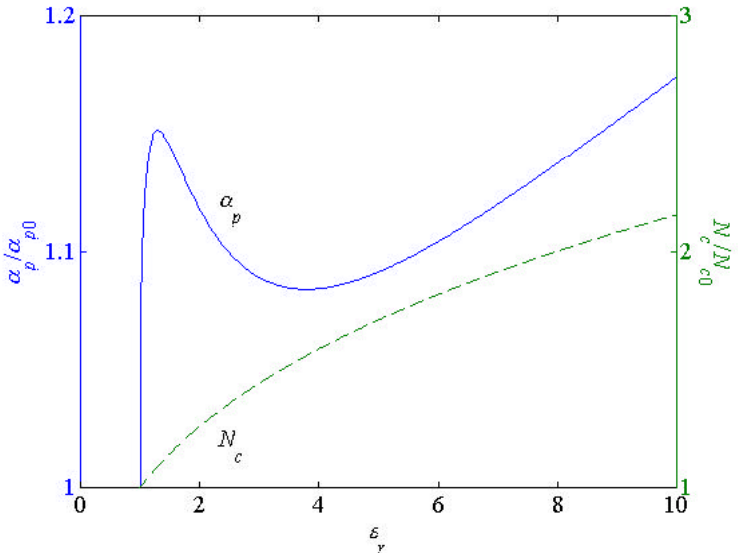

Figure 7. Relative momentum compaction, a_p/a_{p0}, and relative number of TME-cells per arc, N_c/N_{c0}, plotted as a function of the 'detuning' factor, e_r. The normalization of these relative curves is with respect to their values at $e_r = 1$ [*i.e.* $a_{p0} \equiv a_p(e_r=1)$ and $N_{c0} \equiv N_c(e_r=1)$].

2.13 Choice of Wiggler Length

The choice of relative wiggler strength, F_w, involves, in part, evaluating Eqs. (9), (12), (30) and (32) [*i.e.* damping time, wiggler length, number of cells and momentum compaction]. If the arc bends are to have fields of $B_a < 18$ kG, then, for the MDR parameters of Table 1 at 2 GeV, the wiggler needs $F_w > 1$. The choice of F_w also impacts many other critical ring parameters, such as momentum compaction, as described above.

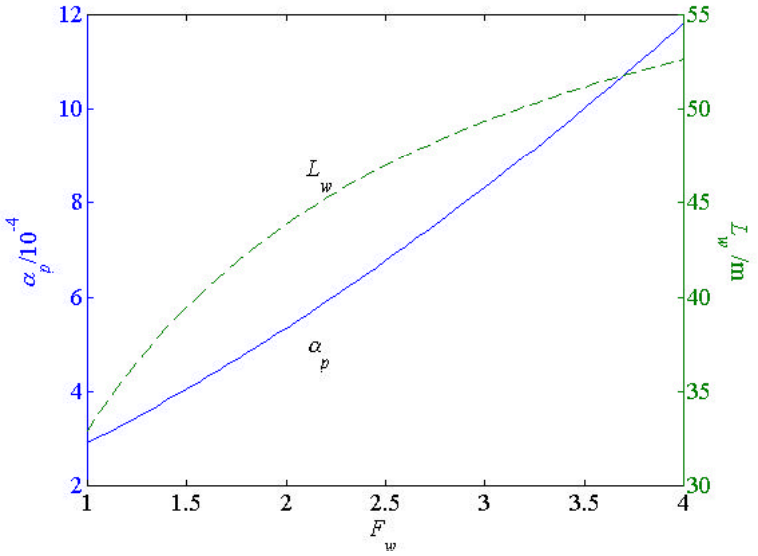

Figure 8. Momentum compaction, a_p, and wiggler length, L_w, plotted versus wiggler damping, F_w.

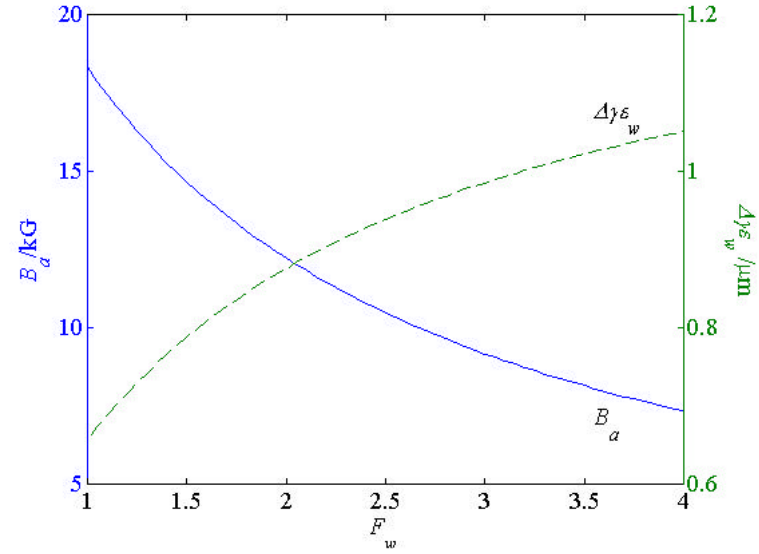

Figure 9. Arc dipole field, B_a, and wiggler's emittance contribution, $\Delta\gamma\varepsilon_w$, plotted against F_w.

Figure 8 and Figure 9 show the momentum compaction, a_p, active wiggler length, L_w, arc dipole field, B_a, and the wiggler's contribution to horizontal equilibrium emittance,

$\Delta\gamma\varepsilon_w \equiv g e_w F_w/(J_{x0} + F_w)$, all plotted against the wiggler relative damping factor, F_w. The parameters are those of the MDR at 1.98 GeV and with $C \approx 297$ m, $t_y \approx 5.2$ msec, $l_w = 27$ cm, $\langle b_x \rangle \approx 4.5$ m, $B_w = 21.5$ kG, and $e_r = 1.647$. The momentum compaction increases fairly rapidly with F_w while the wiggler length increases asymptotically (Figure 8). The arc dipole fields, B_a, are reasonable, at 2 GeV, for $F_w > 1$, but the wiggler's contribution to the horizontal equilibrium emittance increases with increasing F_w (Figure 9). An increase in emittance requires reducing the arc bend angles by adding TME cells.

In longitudinal phase space, the rms extracted relative energy spread, s_d, and rms bunch length, s_z, (for zero current) are given by

$$s_d = \sqrt{\frac{C_q I_3}{2I_2 + I_4}} \approx g \left[\frac{C_q B_a}{(Br)} \cdot \frac{1 + F_w B_w / B_a}{3 - J_{x0} + 2F_w} \right]^{1/2}, \tag{33}$$

$$s_z \approx C s_d \sqrt{\frac{a_p g\, mc^2}{2p\, heV_0 |\cos j_0|}}, \tag{34}$$

where h ($= f_{RF} C/c$) is the ring's harmonic number, V_0 is the on-crest RF voltage in the ring, and j_0 is the synchronous RF phase angle given by

$$j_0 \approx \sin^{-1}\left(\frac{2Cg\, mc^2}{ct_y eV_0} \right). \tag{35}$$

The extracted energy spread and bunch length are plotted in Figure 10 as a function of F_w using MDR parameters of Figure 8 and Figure 9, B_a from Eq. (9), a_p from Eq. (32), $V_0 = 1.5$ MV, and $h = 708$.

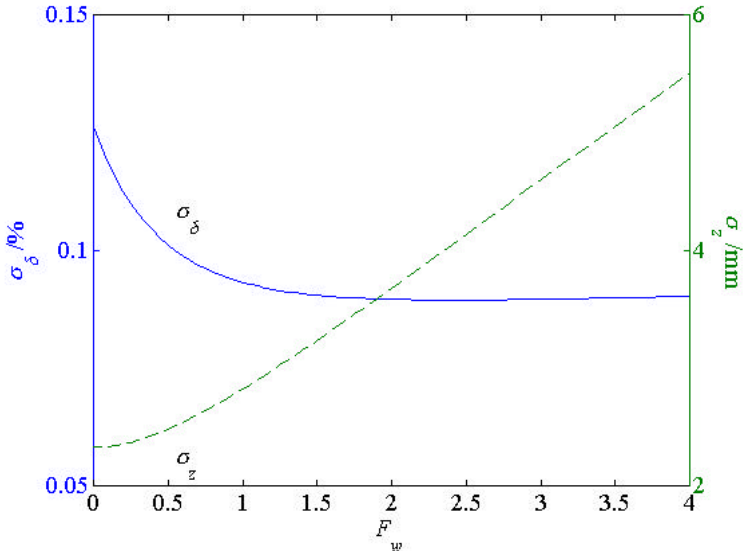

Figure 10. MDR extracted energy spread, s_d, and bunch length, s_z, plotted against F_w.

For the MDR design, a value for $F_w = 2.3$ is chosen in order to keep $a_p > 5\times10^{-4}$ and to produce a bunch length of 4 mm rms at $V_0 = 1.5$ MV. The active wiggler length at $F_w = 2.3$ is then $L_w \approx 46$ m and the arc bend fields are a modest 11 kG.

2.14 Design Completion

With the choices made for F_w and e_r, the remainder of the ring can be laid out. The length of a TME-cell, L_c, is calculated (for the MDR) using

$$L_c = \left(C/2 - L_w - \Delta L\right)/N_c \,, \tag{36}$$

where ΔL (> 0) is an additional straight section length which is included in order to provide space for the arc-to-straight matching sections and for the FODO-cell quadrupole magnets located between modular wiggler segments. In the MDR the wiggler is situated fully on one side of the ring while the PDR includes a half-length wiggler on each side of the ring. This allows more room for the optics surrounding the more challenging PDR injection kicker, with its very large incoming e^+ beam size, and for the MDR, puts the injection and extraction systems on the opposite side of the ring from the wiggler (see Figure 11 and Figure 12).

The length of the modular wiggler segments and the length of the drifts between segments must be determined with a detailed wiggler design. For this study we assume a 2.3-m wiggler segment length and a 36-cm inter-segment drift space which includes a 15-cm long quadrupole magnet. The wiggler then requires 20 segments. This sets a lower limit on ΔL of 20×0.36 m = 7.2 m. The final value of ΔL is set by considering the space required for the matching sections. This is arrived at by running the computer program MAD [10] which minimizes the quadrupole strengths and beta functions through the matching sections. For the NLC MDR, a value of $\Delta L \approx 12.2$ m is used. The TME-cell length is then 6.0 m with 15 cells per arc. This generates an equilibrium horizontal emittance of $ge_x \approx 3.0$ mm [see Eq. (28)]. With the cell length known, the TME-cell is fitted using a 3-quadrupole cell (as in Figure 5) constraining the cell phase advances, and the dispersion and beta functions of Eq. (24) at the bend center. For the MDR, the quadrupole pole-tip fields are very reasonable at 5.9 and –4.6 kG for 25-cm long magnets with 20 mm radii. In contrast, the PDR TME cells are formed using four quadrupole magnets as shown in Figure 6. This reduces the peak value of the beta functions which, with the very large input emittance of the PDR, better controls the peak transverse beam size through the arcs.

This leads back into the argument for the MDR selection of $N_t = 3$ bunch trains. If the MDR is re-designed with $N_t = 2$ trains, the circumference is reduced to 198 m, but the cell length is reduced to 2.8 m. The 2-train MDR is designed for the same momentum compaction as the 3-train MDR (by reducing $F_w = 1.7$), which keeps the wiggler length

nearly constant, but the same length and radii quadrupole magnets now require pole-tip fields >12 kG. The dispersion in the sextupoles is also reduced and so it is expected that the dynamic aperture will suffer. For these reasons we choose $N_t = 3$ bunch trains for the MDR and $N_t = 2$ bunch trains for the PDR. A list of MDR and PDR parameters is given in Table 2. A list of various magnet parameters is also included in Table 3 and the entire MDR and PDR rings are shown in Figure 11 and Figure 12, respectively.

Table 2. List of NLC MDR and PDR parameters for collider parameters of Table 1.

parameter	symbol	PDR	MDR	unit
nominal electron/positron ring energy	gmc^2	1.98	1.98	GeV
Number of bunch trains stored	N_t	2	3	m
Store time/train in units of damping time const.	N_t	3.1	4.8	m
ring circumference	C	218	297	m
ratio of *y*-equilibrium to *y*-extracted emittance	e_{ye}/e_y	0.1	0.67	
extracted horizontal emittance (norm., rms)	ge_x	150	3	mm
extracted vertical emittance (norm., rms)	ge_y	100	0.03	mm
vertical damping time ($t_y \approx t_x$)	t_y	5.4	5.2	msec
ratio of energy loss in wiggler to that in arcs	F_w	0.5	2.3	
peak field of wiggler	B_w	21.0	21.5	kG
wiggler period	l_w	100	27	cm
net active wiggler length (not inc. segment gaps)	L_w	16	46	m
emittance detuning factor	e_r	1.65	1.65	
momentum compaction	a_p	40	6.6	10^{-4}
harmonic number	h	520	708	
extracted energy spread (rms)	s_d	8.9	8.9	10^{-4}
energy loss per turn	U_0	0.53	0.76	MeV
extracted bunch length (rms @ $V_0 = 1.5$ MV)	s_z	8.1	4.0	mm
Number of quadrupole magnets per TME-cell		4	3	
Number of TME-cells/arc ($N_c - 1$ *full* cells/arc)	N_c	6	15	mm
TME-cell length	L_c	11	6.0	m

It should be noted that the MDR energy can be increased to 2.8 GeV and attain the necessary damping and emittance values while eliminating the need for a wiggler altogether. This is an interesting possibility, but in this case the momentum compaction for a 3-train MDR ring is reduced to 1.6×10^{-4}, which is thought, at the present time, to be too small. The higher energy also forces the number of cells to be doubled (*i.e.* 30 per arc) and pushes the energy loss per turn above 1 MeV. The TME quadrupoles also require nearly twice the field strength and the dispersion in the sextupoles is reduced due

to the shorter cells. For these reasons, we choose an energy of 1.98 GeV for both rings which requires a wiggler in each ring.

Table 3. List of various magnet parameters in the NLC MDR and PDR.

parameter	symbol	PDR	MDR	unit
length of arc dipole magnet (full length)	L	2.01	1.23	m
field of arc dipole magnets (full & half length)	B_a	17.2	11.25	kG
bend angle of full length dipole magnets	q	30	12	deg
length of arc quadrupole magnets	L_{Q}	0.30	0.25	m
pole-tip radius of arc quadrupole magnets	r_{Q}	50	20	mm
field of QF (inner) arc quadrupole magnets	B_{QF}	+7.2	+5.9	kG
field of QD (outer) arc quadrupole magnets	B_{QD}	–3.9	–4.6	kG

Title:
mad.metafile.ps
Creator:
gx11 version 1.50
Preview:
This EPS picture was not saved
with a preview included in it.
Comment:
This EPS picture will print to a
PostScript printer, but not to
other types of printers.

Figure 11. Optical functions of the entire MDR. The wiggler is the darkened area at $s \approx$ 50-100 m.

Figure 12. Optical functions of the entire PDR. The wigglers are the two darkened areas.

Alternate ring layouts can also be explored. One possibility is a 'dog-bone' ring where each arc includes 360° of bending [12], rather than the race-track with 180° per arc. The increased bending can be used to eliminate the wiggler, even at 2 GeV. Unfortunately, the number of TME cells more than doubles and the cell lengths are halved. In the MDR, this forces unrealistically strong quadrupole strengths, small dispersion in the sextupoles and a momentum compaction value of $\sim 4\times10^{-4}$. This scheme has been discarded.

Finally, tunable 4-dipole chicanes have been added to the straight sections to allow empirical corrections of the ring circumference (at $s \sim 200$ m in Figure 11, and $s \sim 40$ m in Figure 12) [13]. Since the ring RF frequency needs to be locked to the extraction linac, we employ a magnetic chicane to make small circumference corrections against possible ground motion or temperature induced variations. The critical ring parameters are not significantly affected by the chicanes.

3 Conclusions

The design for a damping ring using TME-cells can be fairy well determined by the emittance reduction requirements, the collider repetition rate, the number and spacing of the bunches in a train, and kicker bandwidth limitations. Other concerns such as momentum compaction, wiggler length, bunch length, and limiting the number of components can be included to produce a relatively unique design. A computer program has been written to quickly generate complete ring parameter sets for various collider and injector schemes. The choice of tunes and type of sextupole compensation is best left to future dynamic aperture studies. Collective effects have not been considered here.

4 References

[1] *Zeroth-order Design Report for the Next Linear Collider*, SLAC-REP-474, May 1996.

[2] L. C. Teng, LS-17 1985, ANL-FNAL.

[3] T. O. Raubenheimer, L. Z. Rivkin, R. D. Ruth, *Damping Ring Designs for a TeV Linear Collider,* SLAC-PUB-4808, December 1988.

[4] T. O. Raubenheimer, *The Generation and Acceleration of Low Emittance Flat Beams for Future Linear Colliders*, SLAC-387, November 1991.

[5] R. Helm, et al., *Evaluation of Synchrotron Radiation Integrals*, SLAC-PUB-1193, March 1973.

[6] J.P. Potier, L. Rivkin, *A Low Emittance Lattice for the CLIC Damping Ring*, CERN-PS-97-020, May 1997.

[7] Field gradients in the bends have been included in the analysis and design of several alternate versions of the MDR lattice with little clear benefit and so have been eliminated in this ‘final’ version.

[8] L. Rivkin, *The 7th International Workshop on Linear Colliders* (LC97), Zvenigorod, Russia; Sep.-Oct. 1997, pp. 644.

[9] K. Halbach, J. Appl. Phys. 57, 3605 (1985).

[10] H. Grote, F.C. Iselin, *The MAD Program*, CERN/SL/90-13 (AP) Rev. 3 (1993).

[11] This was studied numerically and an approximate analytical argument was provided by J. Murphy at BNL, 1999.

[12] This idea was suggested by Bobby McKee, SLAC; 1999.

[13] P. Emma, T. O. Raubenheimer, *Circumference Correction Chicanes for Damping Rings*, 1999 IEEE Particle Accelerator Conference (PAC99), New York, NY, Vol. 5 pp. 3438-3440.